



Comparison of the multi-configuration, time-dependent Hartree (MCTDH) method with the Arthurs and Dalgarno coupled-channel method for rotationally inelastic scattering



R.F. Malenda^{a,1}, F. Gatti^b, H.-D. Meyer^c, D. Talbi^d, A.P. Hickman^{a,*}

^a Department of Physics, Lehigh University, 16 Memorial Dr. East, Bethlehem, PA 18015, USA

^b CTMM, Institut Charles Gerhardt, UMR 5253, Université Montpellier II, Place Eugène Bataillon, 34095 Montpellier, France

^c Theoretische Chemie, Physikalisch-Chemisches Institut, Universität Heidelberg, Im Neuenheimer Feld 229, D-69120 Heidelberg, Germany

^d Laboratoire Univers et Particules de Montpellier, UMR 5299, Université Montpellier II, Place Eugène Bataillon, 34095 Montpellier, France

ARTICLE INFO

Article history:

Received 27 May 2013

In final form 19 August 2013

Available online 24 August 2013

ABSTRACT

Calculations of rotationally inelastic scattering at thermal energies for a model atom–diatom system have been performed using two completely different methodologies. The first method is the multi-configuration time-dependent Hartree (MCTDH) wave packet method, and the second is the well known, time-independent, Arthurs and Dalgarno coupled channel formalism. Excellent agreement is obtained between the two calculations. The advantages and drawbacks of these two methods are somewhat complementary, so that the decision to use one or the other approach will depend on what type of computational results are desired.

© 2013 Elsevier B.V. All rights reserved.

1. Introduction

The development in the last few years of the multi-configuration, time-dependent Hartree (MCTDH) method [1–3] for wave packet propagation has enabled a large variety of molecular processes to be modeled accurately and efficiently. The MCTDH method has been applied to photoexcitation [4], photodissociation [5], ro-vibrational excitation [6], and reactive and non-reactive scattering [7–9]. Multiple electronic states may be included. Previous studies have confirmed the accuracy of MCTDH calculations for vibrational energy levels [10], for dynamics in the presence of an external time-dependent field [11], and for reactive collisions of H + H₂ (or D₂) [12]. In the present letter, we present a systematic comparison of the results obtained for rotationally inelastic scattering with the Heidelberg MCTDH package [13] with those obtained by a completely different method.

The scattering process considered in this letter exhibits different features from the systems studied previously with MCTDH and thus provides a nontrivial test. For most previous work with MCTDH, the masses of the atoms involved (H, D, O, C, N, etc.) have been rather small. Here we focus on the delicate process of rotational excitation of heavier molecules. The energy level splittings are very small, and consequently the change $\Delta j = j' - j$ of the angular

momentum quantum number in a collision can be fairly large. In addition, there are long range terms in the potential that enhance the importance of trajectories with very large impact parameters. We have compared the results of MCTDH with the traditional, coupled channel [CC] method [14] for this process. Since both methods are, at least in principle, exact methods of solving the Schrödinger equation, one expects agreement. However, achieving agreement in practice required that the scattering simulations with MCTDH be very carefully designed. For example, we found it necessary to adjust some details of the MCTDH calculations when the total angular momentum of the propagation was large. We also paid particular attention to the choice of parameters for the complex absorbing potentials (CAPs) to insure accurate monitoring of fluxes. The experience we have gained should facilitate the application of the MCTDH method to other scattering problems.

This letter is organized as follows. Section 2 describes briefly the MCTDH approach. Section 3 summarizes our application of MCTDH to calculate cross sections for rotational excitation. We used the masses of the He–NaK molecule and an analytic model potential that roughly represents the ground electronic state of He–NaK. Section 4 describes the coupled channel calculations. Finally, section 5 compares the results of the two methods and discusses the pros and cons of each method.

2. The MCTDH approach

In a conventional propagation method, the wave function is directly expressed in the mathematical or ‘primitive’ basis set:

* Corresponding author. Fax: +1 610 758 5730.

E-mail addresses: ruth.malenda@gmail.com (R.F. Malenda), gatti@univ-montp2.fr (F. Gatti), Hans-Dieter.Meyer@pci.uni-heidelberg.de (H.-D. Meyer), dahbia.talbi@univ-montp2.fr (D. Talbi), aph2@lehigh.edu (A.P. Hickman).

¹ Current address: Department of Physics, Moravian College, 1200 Main St., Bethlehem, PA 18018, USA.

$$\Psi(Q_1, \dots, Q_f, t) = \sum_{j_1=1}^{N_1} \dots \sum_{j_f=1}^{N_f} L_{j_1 \dots j_f}(t) \prod_{\kappa=1}^f \chi_{j_\kappa}^{(\kappa)}(Q_\kappa), \quad (1)$$

where Q_1, \dots, Q_f denote the f nuclear coordinates, N_1 the number of primitive functions for degree of freedom l , $\chi_{j_\kappa}^{(\kappa)}$ are the ‘primitive’ time-independent functions, typically Hermite functions, spherical harmonics, or the functions associated with a Discrete Variable Representation (DVR). The equations of motion for the coefficients $L_{j_1 \dots j_f}(t)$ can be derived from the Dirac-Frenkel variational principle, i.e. by minimization of $\langle \delta\Psi | H - i\partial_t | \Psi \rangle = 0$.

In contrast, the wave function in the MCTDH approach is written as follows [2]:

$$\Psi(Q_1, \dots, Q_f, t) \equiv \Psi(q_1, \dots, q_p, t) = \sum_{j_1=1}^{n_1} \dots \sum_{j_p=1}^{n_p} A_{j_1 \dots j_p}(t) \prod_{\kappa=1}^p \varphi_{j_\kappa}^{(\kappa)}(q_\kappa, t) \quad (2)$$

q_1, \dots, q_p are ‘logical’ coordinates that can be either nuclear coordinates or sets of nuclear coordinates combined together (combined modes). The $\varphi_{j_\kappa}^{(\kappa)}(q_\kappa, t)$ are the so-called single-particle functions (SPFs), which are in turn expressed in the primitive basis set:

$$\varphi_{j_\kappa}^{(\kappa)}(Q_\kappa, t) = \sum_{i_\kappa=1}^{N_\kappa} G_{i_\kappa}^{j_\kappa}(t) \chi_{i_\kappa}^{(\kappa)}(Q_\kappa). \quad (3)$$

The equations of motions of the coefficients $A_{j_1 \dots j_p}(t)$ and of the single-particle functions $\varphi_{j_\kappa}^{(\kappa)}(q_\kappa, t)$ (i.e. the equations of motions of the coefficients $G_{i_\kappa}^{j_\kappa}(t)$) are obtained using the Dirac-Frenkel variational principle. In other words, the difference between the MCTDH and the conventional propagation methods is the fact that, in MCTDH, the wave function is expressed in an intermediate time-dependent basis set that is optimized by a variational principle. In general, $n_1 \times \dots \times n_p$ is significantly smaller than $N_1 \times \dots \times N_f$.

3. Rotationally inelastic scattering with MCTDH

We will apply the MCTDH method to the model atom-diatom system illustrated in Figure 1. We assume that the internuclear separation of the target, r , has a fixed value, so that the interaction potential V depends only on R and θ . The Hamiltonian for this system [15] has the form

$$\hat{H} = \frac{\hbar^2}{2\mu} \left(-\frac{\partial^2}{\partial R^2} + \frac{J(J+1) - 2K^2 + j^2 - A_+ \hat{j}_+ - A_- \hat{j}_-}{R^2} \right) + B j^2 + V(R, \theta), \quad (4)$$

where

$$A_\pm \hat{j}_\pm = \sqrt{J(J+1) - K(K \pm 1)} \left(\pm \frac{\partial}{\partial \theta} - K \cot \theta \right), \quad (5)$$

and μ is the reduced mass of the atom–target system,

$$\mu = \frac{m(M_1 + M_2)}{m + M_1 + M_2}. \quad (6)$$

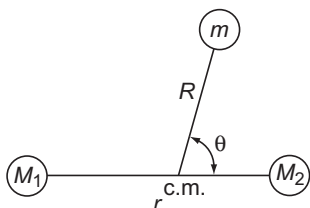


Figure 1. Illustration of the coordinates used for the atom–diatom system. For the present work, we assume that the internuclear separation r of the diatom is fixed. The abbreviation ‘c.m.’ denotes the center of mass of the diatom.

K is the projection of the total angular momentum J onto R . B is the rotational constant,

$$B = \frac{\hbar^2}{2\mu_r r^2}, \quad (7)$$

where

$$\mu_r = \frac{M_1 M_2}{M_1 + M_2}. \quad (8)$$

A separate wave packet propagation must be carried out for each value of J and for each initial rotational state (j, m) .

For the interaction potential V , we used the general form

$$V(R, \theta) = \sum_{\lambda} V_{\lambda}(R) P_{\lambda}(\cos \theta). \quad (9)$$

This form is well suited for MCTDH because the algorithms used in the code are most efficient when the Hamiltonian can be written as sums of products of mono-mode operators. In fact, this form is optimal for any quantum method when the evaluation of matrices is necessary since this form allows one to express any multi-dimensional integral as a sum of products of low-dimensional integrals. This is particularly important if the number of degrees of freedom is large (more than six, typically). The whole Hamiltonian, Eq. (4), as well as the potential, Eq. (9), satisfy this condition. For the purposes of the present study, we used a simple analytic form for the V_{λ} coefficients:

$$V_{\lambda}(R) = a_{\lambda} \exp(-b_{\lambda} R). \quad (10)$$

We obtained the parameters a_{λ} and b_{λ} by performing small *ab initio* electronic structure calculations for the He–NaK molecule at several representative geometries using the GAMESS code [16]. For these calculations the internuclear separation of NaK was fixed at its equilibrium values, so the rigid-rotor potential thereby determined should be appropriate for the $v = 0$ vibrational level. At several values of R we fit the calculations using five-term Legendre fits, thereby determining a table of numerical values of $V_{\lambda}(R)$ for $\lambda = 0, 1, \dots, 4$. We then fit the numerical values of each $V_{\lambda}(R)$ using the analytic form in Eq. (9). The values obtained are listed in Table 1. This procedure provided a model potential that could be used to compare different computational methods; the potential obtained should not be considered a highly accurate representation of the specific He–NaK molecule.

MCTDH propagates the wave packets using a basis set expansion as shown in Eqs. (2) and (3). For the present case, the target rotational state is expanded in a basis of spherical harmonics, and the built-in Colbert–Miller DVR [17] (also called sine DVR) basis set is used for the R degree of freedom. Details are in Table 2. The system is described by three coordinates: in Eq. (2), $q_1 = Q_1 = R$, $q_2 = (Q_2, Q_3)$ with $Q_2 = \theta$ and $Q_3 = \phi$. In Eq. (3), $N_1 = 863$, $N_2 = 31$, and $N_3 = 61$ (see Table 2). In MCTDH, the wave function is not directly expressed in the primitive basis set but in an intermediate basis set, which is the basis set of the single-particle functions (see Eq. (2)). In our case, we have chosen $n_1 = 20$ and $n_2 = 20$ (see Table 2). It is worth noting that the ratio $r_{\text{MCTDH}} = n_1 \times n_2 / (N_1 \times N_2 \times N_3) = 400/1631933$ shows that MCTDH allows one to drastically reduce the number of basis

Table 1
Values of the constants used for the exponential functions in the model potential.

λ	a_{λ}	b_{λ}
0	1.26100	0.798340
1	−0.99356	0.752171
2	0.8018727	0.717405
3	−1.0	0.817900
4	1.0	0.879588

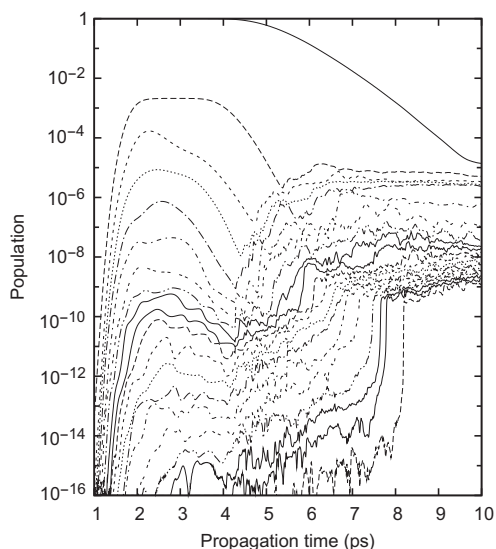
Table 2

Parameters for the primitive basis set and the number of single particle functions (SPF) employed for each degree of freedom. sine-DVR denotes the sine discrete variable representation of Colbert and Miller [17]. The extended Legendre DVR KLeg uses the spherical harmonic basis functions. K is the projection of the angular momentum on the body-fixed z axis.

	R	θ, ϕ
Primitive basis	Sine-DVR	KLeg-DVR
Number of points or functions	863	$j = 0, 1, \dots, 30$ for θ and $K = -30, -29, \dots, 30$ for ϕ
Range	8.0–79.0 a_0	0– π for θ and 0– 2π for ϕ
Size of SPF basis	20	20

functions with respect to conventional propagation methods. Figure 2 displays the populations of the natural single-particle functions for the two combined modes R as a function of time. The corresponding figure for the second mode (θ, ϕ) looks similar. This allows us to estimate the convergence behavior of the MCTDH approach. In general, it is considered that the convergence is reached when the last population is smaller than 10^{-4} . Figure 2 clearly shows that with 20 SPFs, MCTDH has reached a very high level of convergence. The last population (the 20th) is of order 10^{-9} . It could be possible to work with smaller values of n_1 and n_2 and to reduce the ratio r_{MCTDH} even more (here only four SPFs would be sufficient). This will be important when we add more degrees of freedom in our simulations. But even with $n_1 = n_2 = 20$, the MCTDH calculations were about a factor of two faster than the CC calculations. (More details are given in Section 5.)

The initial wave packet is a gaussian, specified by a position, width and momentum. The initial momentum of the incident particle He (in the center of mass frame) was exactly 4.0 a.u., which is nominally equivalent to an energy of 0.00116706 E_h . In principle, this initial wave packet should start at infinity and undergo free motion towards the scattering center. To simulate this motion, an ‘adiabatically corrected’ [2] wave packet can be started closer to the scattering center; the correction accounts for propagation from infinitely far away. The interaction at the initial position must be small enough to ensure that this correction is accurate. After careful testing, we found that a starting position at $R = 64.0 a_0$ was sufficiently far from the scattering center. This is why we have chosen a large range for R (8.0–79.0 a_0). Such a long range was necessary since the large values of J create a long range centrifugal potential and the initial wave packet must start at large values of R .

**Figure 2.** The population of the natural single-particle functions for R .

Since the adiabatic correction depends on J , the initial wave packets are different for each value of J and correspond to slightly different distributions $\Delta^J(E)$ of initial translational energies. These distributions are shown in Figure 3 for several different values of J . The dependence on J is negligible for small J but becomes increasingly stronger for larger J . Since many large values of J contribute to the scattering, it is important to determine $\Delta^J(E)$ accurately for the propagation for each J . We did this using the autospec routine (from the MCTDH package [13]), which evaluates the Fourier transform of the autocorrelation function determined during a short time interval at the beginning of the propagation. (The interval must be long enough so that the autocorrelation function has time to decrease to zero.) For each J , the energy distribution $\Delta^J(E)$ and the quantum flux in each channel determine transition probabilities, as described in the next paragraph.

MCTDH, like any wave packet propagation scheme, implements a complex absorbing potential (CAP) near the end of the R grid. This CAP absorbs the wave packet as it approaches the edge of the grid and eliminates unphysical reflections. The CAP is also used to determine the quantum flux. As the scattered wave packet propagates outward through the CAP, MCTDH determines the contribution of each final state of the system to the absorption; this contribution is the quantum flux for each final state. Transition probabilities between specific initial and final states are found by dividing the corresponding flux by the energy distribution, $\Delta^J(E)$. The CAP turns on gradually for large values of R ; the analytic form is [15]

$$-iW(R) = -i\eta|R - R_0|^b\Theta(R - R_0), \quad (11)$$

where R_0 , η , and b are the starting point, the strength, and the order of the CAP, respectively, and Θ is the Heaviside step function. The MCTDH program has built-in routines to determine which CAP parameters are best suited for a particular calculation. We used these routines to determine appropriate parameters, which are tabulated in Table 3.

Each separate wave packet propagation models the scattering, for a fixed J , from a particular initial state (j, m_j) to several possible final states (j', m_j'). A specific transition probability is denoted $P^J(j, m \rightarrow j', m_j')$. By performing propagations for many values of J , one can compute total cross sections as a sum:

$$\sigma_{j, m_j \rightarrow j', m_j'}^{\text{BF}}(E) = \frac{\pi}{(2j+1)k_j^2} \sum_J (2J+1) P^J(j, m_j \rightarrow j', m_j'). \quad (12)$$

We use the superscript ‘BF’ to emphasize that the m quantum numbers are determined in the body frame, that is, with respect to the rotating collision axis. E , the total energy of the system, is the

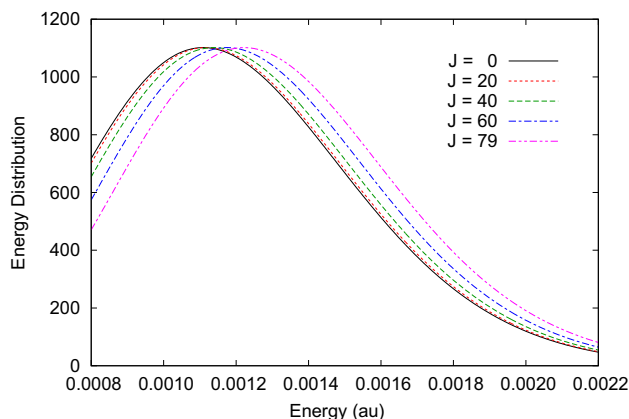
**Figure 3.** This figure shows the energy distribution $\Delta^J(E)$ for several different values of J for the adiabatically corrected initial wave packet.

Table 3

Values of the parameters used for the Complex Absorbing Potential.

Parameter	Value
R_0	69.0 a_0
η	$4.3824 \times 10^{-6} E_h/a_0$
b	4

sum of the relative translational energy and the internal energy of the target, and one has

$$k_j^2 = \frac{2\mu}{\hbar^2} [E - B_j(j+1)]. \quad (13)$$

Because of the Fourier-transform relation between coordinate and momentum wave functions, one can regard the initial time-dependent wave packet as a superposition of momentum states. Each propagation therefore provides information about a range of translational energies. To determine cross sections for a specific ($j \rightarrow j'$) transition, one must perform propagations for every possible initial m value, and then average over the initial m values and sum over the final m' values:

$$\sigma_{j \rightarrow j'}(E) = \frac{1}{2j+1} \sum_{m'=-j'}^{j'} \sigma_{jm \rightarrow j'm'}^{\text{BF}}(E). \quad (14)$$

4. Coupled-channel method

This section briefly summarizes the CC method for scattering of an atom by a rigid rotor developed by Arthurs and Dalgarno [14], using a notation consistent with Section 3. This method uses a coupled angular momentum representation in a space-fixed coordinate system. Spherical harmonic target states $Y_{jm_j}(\hat{\mathbf{r}})$ of a rigid rotor are combined with orbital angular momentum states of the incident particle and the target, $Y_{lm_l}(\hat{\mathbf{R}})$. Using the coupling scheme

$$\mathbf{j} + \mathbf{l} = \mathbf{J}, \quad (15)$$

basis functions $\mathcal{Y}_{jJM}(\hat{\mathbf{r}}, \hat{\mathbf{R}})$ of total angular momentum J can be defined by appropriate linear combinations of the product states $Y_{jm_j}(\hat{\mathbf{r}})Y_{lm_l}(\hat{\mathbf{R}})$. For each value of the total angular momentum quantum number J , the total wave function is expanded as

$$\Psi_{JMl}(\mathbf{R}, \hat{\mathbf{r}}) = \frac{1}{R} \sum_{j'} \sum_{l'} F_{j'l',jl}^J(R) \mathcal{Y}_{j'l'JM}(\hat{\mathbf{r}}, \hat{\mathbf{R}}). \quad (16)$$

One must then solve the following set of coupled equations for the $F_{j'l',jl}^J(R)$ [14]:

$$\left[\frac{d^2}{dR^2} + k_j^2 - \frac{l'(l'+1)}{R^2} \right] F_{j'l',jl}^J(R) = \frac{2\mu}{\hbar^2} \sum_{\lambda} V_{\lambda}(R) \sum_{j''} \sum_{l''} f_{j'l',j''l''}^{J\lambda} F_{j''l'',jl}^J(R), \quad (17)$$

where the $f_{j'l',j''l''}^{J\lambda}$ may be written in terms of 3- j and 6- j coefficients [14].

We solved these equations using our standard code [18], which is based on the log derivative method [19] and features adaptive step size selection. Solutions can be found that satisfy the boundary conditions

$$\lim_{R \rightarrow \infty} F_{j'l',jl}^J(R) = \delta_{jj'} \delta_{ll'} k_j^{1/2} R j_l(k_j R) + k_j^{1/2} R K_{j'l',jl}^J n_l(k_j R), \quad (18)$$

where j_l and n_l are regular and irregular spherical Bessel functions, respectively, and the $K_{j'l',jl}^J$ are the elements of the reactance matrix \mathbf{K} . The transition matrix \mathbf{T} is related to \mathbf{K} by

$$\mathbf{T} = -2i\mathbf{K}(\mathbf{1} - i\mathbf{K})^{-1}. \quad (19)$$

Then cross sections for transitions from the state j to the state j' , averaged over initial m and summed over final m' , are defined as

$$\sigma_{j \rightarrow j'}(E) = \frac{\pi}{(2j+1)k_j^2} \sum_{l=|j-j|}^{J+j} \sum_{l'=|j'-j|}^{J+j'} (2J+1) |T_{jl'j'l}^J|^2. \quad (20)$$

Eqs. (14) and (20) give the results we compare for the CC and MCTDH calculations. Since all values of m are included in the sum over body-frame cross sections in Eq. (14), the cross section is equivalent to the space-fixed sum in Eq. (20).

5. Comparison of MCTDH and coupled channel results

This section compares the results from the wave packet and coupled channel methods. All MCTDH calculations were performed for an initial momentum of 4.0 a.u., as discussed in Section 3. We analyzed the results to determine cross sections for total energies 0.0008, 0.0011, 0.0014, and 0.0017 E_h . These energies are in the middle portions of the distributions shown in Figure 3. We summed over all values of J from 0 to 79; this range was enough for convergence. To simplify the bookkeeping, we assumed that the initial rotational level was $(j, m) = (0, 0)$. Coupled channel calculations were also performed at energies of 0.0008, 0.0011, 0.0014, and 0.0017 E_h . All rotor states $j = 0 - 28$ were included; this was enough to ensure convergence of cross sections from $j = 0$ up to $j' = 10$.

All of the results are tabulated in Table 4 and shown graphically in Figure 4. Excellent agreement is achieved at all energies. We now discuss several interesting points that emerge when we compare the two calculations.

Table 4

Values of the cross sections $\sigma_{0 \rightarrow j'}$ obtained by the multi-configuration time-dependent Hartree (MCTDH) and the coupled channel (CC) methods.

j'	$E = 0.0008E_h$		$E = 0.0011E_h$		$E = 0.0014E_h$		$E = 0.0017E_h$	
	MCTDH	CC	MCTDH	CC	MCTDH	CC	MCTDH	CC
1	80.94	80.20	78.44	78.42	77.42	77.51	76.63	76.26
2	66.28	65.08	59.03	57.74	55.48	53.76	52.84	50.17
3	88.18	87.74	84.58	82.19	80.16	77.33	77.13	74.07
4	18.14	18.21	18.59	19.68	19.39	20.75	19.74	22.58
5	30.24	29.98	26.64	26.15	23.77	22.67	20.86	19.90
6	31.99	32.41	29.78	31.00	29.09	32.05	28.52	31.35
7	11.21	11.23	10.80	11.28	10.28	11.08	9.77	12.13
8	19.90	20.02	17.71	17.41	15.17	15.35	13.91	13.95
9	12.55	12.70	13.55	14.62	13.35	14.50	12.26	14.33
10	9.52	9.53	8.78	8.49	8.03	7.69	7.44	7.38

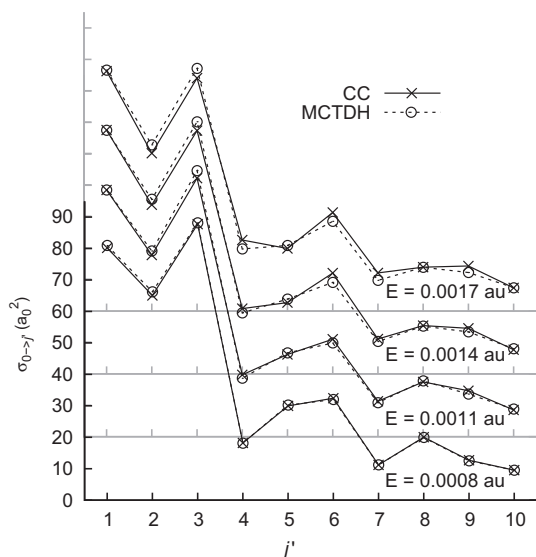


Figure 4. This figure shows the comparison of the cross sections $\sigma_{0 \rightarrow j'}$ obtained by the two different methods for $E = 0.0008, 0.0011, 0.0014,$ and $0.0017 E_h$. The curves for $E = 0.0011, 0.0014,$ and $0.0017 E_h$ have been displaced upward by 20, 40, and 60 a_0^2 , respectively.

First, each propagation in MCTDH provides information about a range of collision energies, whereas a separate CC calculation is necessary for each distinct total energy. This feature of MCTDH might make that method more attractive for the calculation of rate constants, which require a convolution over translational energies.

Second, one CC calculation provides cross sections at a single total energy E for all possible initial states (limited only by the number of channels included in the calculation, and of course, one must sum over J .) For MCTDH, one can pick the initial state, and only perform calculations for that initial state, again summing over J . In the present work, we chose $(j, m) = (0, 0)$, so we only needed to perform propagations for one initial state. We performed a few tests with nonzero initial j . In these cases, careful scripting was implemented to handle the extra bookkeeping. In addition, calculations for many different initial quantum numbers m requires more computer time.

A third point was that the integration range for MCTDH was much larger than for the CC method. The initial wave packet, ‘adiabatically corrected’ as discussed in Section 3, was started at a value of R large enough that the interaction potential, as well as all the centrifugal terms in Eq. (4), were very small. In the time-dependent calculation, the wave packet moves inward, interacts with the target, and then moves outward again. The CAP is used to extract information about cross sections from the outgoing wave packet. The CC method allows the integration region to be shorter. One starts at small R and integrates outward to values of R large enough that the interaction potential (not including the centrifugal terms) is negligible. At that point, the right hand side of Eq. (17) is effectively zero; the solutions $F_{j'l, j'l}^J(R)$ will have the limiting behavior shown by Eq. (18), and the reactance matrix \mathbf{K} can be determined. Typically we integrated out to about 25 a_0 in the CC calculations, whereas the integration grid for MCTDH extended to 79 a_0 .

We did not make a precise comparison of the speed of the two methods because different computers were used for the two sets of calculations, but MCTDH is certainly faster. Roughly speaking, an MCTDH propagation for a single value of J and a single initial rotational state $|jm\rangle$ took 7–12 h on a serial processor. Higher values of J took more time. The total time for all J from 0 to 79 was about 800 h. The coupled channel calculations were typically done on

32–64 processors and took around 1500 processor-hours for the same range of J (about 500 channels for each of two parities, $0 \leq j \leq 30$). Higher values of J took less time because the integration could be started at larger values of R . The coupled channel calculations provided results for all initial rotational states at a given total energy.

In conclusion, we have found near-perfect agreement between two completely different methods of calculating rotational energy transfer. MCTDH is well suited to the case when the initial rotational quantum number is small, because the propagations must only be performed for a few initial states. The ideal case for MCTDH would be when the energy-sudden approximation (negligible rotational state spacing) is valid; then one can construct the cross sections for all $j \rightarrow j'$ transitions using only the results for $\sigma_{0 \rightarrow j'}$ [20,21]. The CC method may be preferred when several initial states need to be considered. However, the number of coupled channels grows very rapidly as more degrees of freedom are included. Generalizing the present CC code to include vibrational as well as rotational motion would increase the computational requirements dramatically and would make the CC calculations prohibitive. In contrast, even though the size of the SPF basis was chosen to obtain a very high level of convergence, the MCTDH calculations were about a factor of two faster than CC. More importantly, the MCTDH program will allow us to treat a larger number of degrees of freedom.

Acknowledgement

R.F.M. and A.P.H. acknowledge support from National Science Foundation (NSF) Grant No. PHY-0652938. D.T. acknowledges support from the French National PCMI program. H.-D.M. and F.G. gratefully acknowledge financial support from the German and French Science Foundations through the common project DFG-Me623/17 and ANR-09-BLAN-0417. Computational facilities at the Pittsburgh Supercomputing Center (PSC) used for this research were supported by NSF through XSEDE resources provided by the XSEDE Science Gateways Program.

References

- [1] H.-D. Meyer, U. Manthe, L.S. Cederbaum, *Chem. Phys. Lett.* 165 (1990) 73–78.
- [2] M.H. Beck, A. Jäckle, G.A. Worth, H.-D. Meyer, *Phys. Rep.* 324 (2000) 1–105.
- [3] H.-D. Meyer, F. Gatti, G.A. Worth (Eds.), *Multidimensional Quantum Mechanics: MCTDH Theory and Applications*, Wiley-VCH, Weinheim, 2009.
- [4] A. Raab, G. Worth, H.-D. Meyer, L.S. Cederbaum, *J. Chem. Phys.* 110 (1999) 936–946.
- [5] U. Manthe, H.-D. Meyer, L.S. Cederbaum, *J. Chem. Phys.* 97 (1992) 3199–3213.
- [6] O. Vendrell, F. Gatti, H.-D. Meyer, *J. Chem. Phys.* 131 (2009) 034308.
- [7] F. Otto, F. Gatti, H.-D. Meyer, *J. Chem. Phys.* 128 (2008) 064305.
- [8] A.N. Panda, F. Otto, F. Gatti, H.-D. Meyer, *J. Chem. Phys.* 127 (2007) 114310.
- [9] S. Bhattacharya, A.N. Panda, H.-D. Meyer, *J. Chem. Phys.* 135 (2011) 194302.
- [10] L. Joubert Dorio, F. Gatti, C. Jung, H.-D. Meyer, *J. Chem. Phys.* 129 (2008) 224109.
- [11] R. Marquardt, M. Sanrey, F. Gatti, F.L. Quere, *J. Chem. Phys.* 133 (2010) 174302, <http://dx.doi.org/10.1063/1.3496374>.
- [12] A. Jäckle, H.-D. Meyer, *J. Chem. Phys.* 109 (1998) 2614–2623.
- [13] G.A. Worth, M.H. Beck, A. Jäckle, H.-D. Meyer, The MCTDH Package, Version 8.2, (2000). H.-D. Meyer, Version 8.3 (2002), Version 8.4 (2007), ML-MCTDH implemented in forthcoming Version 8.5 (2011). Available from: <<http://mctdh.uni-hd.de/>>.
- [14] A.M. Arthurs, A. Dalgarno, *Proc. R. Soc. (Lond.) A Math. Phys. Sci.* 256 (1960) 540–551.
- [15] S. Sukiasyan, H.-D. Meyer, *J. Chem. Phys.* 116 (24) (2002) 10641–10647.
- [16] M.W. Schmidt et al., *J. Comp. Chem.* 14 (1993) 1347–1363.
- [17] D.T. Colbert, W.H. Miller, *J. Chem. Phys.* 96 (1992) 1982–1991.
- [18] A.P. Hickman, D.L. Huestis, R.P. Saxon, *J. Chem. Phys.* 98 (1993) 5419–5430.
- [19] B.R. Johnson, The multichannel log-derivative method for scattering calculations, *J. Comp. Phys.* 13 (1973) 445–449.
- [20] R. Goldflam, S. Green, D.J. Kouri, *J. Chem. Phys.* 67 (1977) 4149–4161.
- [21] M.H. Alexander, S.L. Davis, *J. Chem. Phys.* 78 (1983) 6754–6762.